The Journal of Chemical Physics

Energy dependent parity-pair behavior in NO + He collisions

Cite as: J. Chem. Phys. **149**, 084306 (2018); https://doi.org/10.1063/1.5042074
Submitted: 29 May 2018 . Accepted: 27 July 2018 . Published Online: 24 August 2018

Jolijn Onvlee, Sjoerd N. Vogels, Tijs Karman, Gerrit C. Groenenboom, Sebastiaan Y. T. van de Meerakker, and Ad van der Avoird

Energy dependent parity-pair behavior in NO + He collisions

Jolijn Onvlee,[1,2] Sjoerd N. Vogels,[1] Tijs Karman,[1] Gerrit C. Groenenboom,[1] Sebastiaan Y. T. van de Meerakker,[1] and Ad van der Avoird[1,a)]
[1]*Institute for Molecules and Materials, Radboud University, Heijendaalseweg 135, 6525 AJ Nijmegen, The Netherlands*
[2]*Center for Free-Electron Laser Science, Deutsches Elektronen-Synchrotron DESY, Notkestrasse 85, 22607 Hamburg, Germany*

(Received 29 May 2018; accepted 27 July 2018; published online 24 August 2018)

Colliding molecules behave fundamentally differently at high and low collision energies. At high energies, a collision can be described to a large extent using classical mechanics, and the scattering process can be compared to a billiard-ball-like collision. At low collision energies, the wave character of the collision partners dominates, and only quantum mechanics can predict the outcome of an encounter. It is, however, not so clear how these limits evolve into each other as a function of the collision energy. Here, we investigate and visualize this evolution using a special feature of the differential cross sections for inelastic collisions between NO radicals and He atoms. The so-called "parity-pair" transitions have similar differential cross sections at high collision energies, whereas their cross sections are significantly different in the quantum regime at low energies. These transitions can be used as a probe for the quantum nature of the collision process. The similarity of the parity-pair differential cross sections at high energies could be theoretically explained if the first-order Born approximation were applicable. We found, however, that the anisotropy of the NO–He interaction potential is too strong for the first-order Born approximation to be valid, so higher-order perturbations must be taken into account. *Published by AIP Publishing.* https://doi.org/10.1063/1.5042074

I. INTRODUCTION

Cold and ultracold atoms and molecules have received much attention in chemical, atomic, molecular, and optical physics in the last decades.[1–7] Methods have been developed to cool and slow down species to temperatures below 1 K, ranging from laser cooling and photoassociation to buffer-gas cooling and Stark deceleration, for instance.[8–12] One of the ultimate goals at these low temperatures is to achieve quantum control of atomic and molecular collisions.[13,14]

In these cold and ultracold regimes, collisions between atoms and molecules are completely governed by quantum mechanics and only one or a few individual partial waves determine the collision dynamics. This is completely different from collisions at high temperatures, where many properties of the collision can be understood in terms of classical mechanics and where many partial waves contribute.

The transition from the semiclassical regime at high temperatures to the quantum regime at low temperatures is often hard to grasp, and probing both regimes in one experiment is challenging. Here, we use the so-called "parity-pair" transitions in collisions between NO radicals and helium atoms to investigate the effect of the wave character on the scattering process. We study the collision energy dependence of this effect, starting at high energies and moving toward the quantum regime.

The parity-pair transitions that occur in collisions between NO ($X^2\Pi_{1/2}$, $j = 1/2, f$) radicals in their vibrational ground state ($v = 0$) and rare gas atoms are transitions to j', e and $j' + 1$, f final rotational states that have the same parity $p' = \epsilon'(-1)^{j'-1/2}$, and the same value for $n = j' - \epsilon\epsilon'/2$. Here, j' is the final rotational level of the NO molecule and ϵ and ϵ' are the spectroscopic parity indices of the initial and final state, respectively, where states of e parity have $\epsilon = +1$, while states of f parity have $\epsilon = -1$. As first observed by Stolte and co-workers,[15–17] the differential cross sections (DCSs) for these parity-pair transitions are similar at relatively high collision energies of a few hundred cm^{-1}. This similarity could be explained using the quasi-quantum treatment (QQT).[16] Within this approach, the DCSs for two neighboring rotational states with the same parity p' are similar, except for a different prefactor ($j' + 1/2$). Other observations regarding the similarity of the parity-pair DCSs are discussed in Refs. 18 and 19. A weak coupling, direct Born scattering model that would directly explain the similarity of the DCSs for the parity pair considered in the present paper will be discussed in more detail in Sec. IV B.

Until now, the calculations and experiments for studying parity pairs have been performed at relatively high collision energies >500 cm^{-1}. Here, we study the collision energy dependence of the similarity of DCSs for parity pairs, both experimentally and theoretically. In the experiments, we use a Stark decelerator in combination with a velocity map imaging (VMI) detector. Thus, we obtained a high angular resolution allowing us to investigate the similarity of the parity-pair DCSs

a)Electronic mail: avda@theochem.ru.nl

at the level of diffraction oscillations, which are the narrowest structures that occur in a DCS. We use the $j = 1/2, f \rightarrow j' = 3/2, e$ and $j = 1/2, f \rightarrow j' = 5/2, f$ transitions for NO + He as an example to show that these parity pairs provide a probe for the quantum nature of a scattering process. Theoretically, we study these collisions by means of quantum mechanical close-coupling (QM CC) calculations based on accurate NO–He potential energy surfaces (PES) from *ab initio* electronic structure calculations.

II. METHODS

In the experiment, we used a crossed beam scattering apparatus, in which we produced a well-defined packet of NO ($X^2\Pi_{1/2}$, $v = 0, j = 1/2, f$) radicals with a mean velocity of 390 m/s using a Stark decelerator. These molecules intersected with a beam of He atoms under an angle of 45°. The beam of He atoms was produced by cooling an Even-Lavie valve to a temperature of 30 K. By altering the temperature, we could produce beams of He atoms with a mean velocity ranging from 1710 to 590 m/s and thereby vary the experimental collision energy between 315 and 25.9 cm^{-1}. The scattered molecules were state-selectively detected using a two-color resonance enhanced multiphoton ionization scheme and a VMI detector. A more detailed description of the experimental setup can be found in the supplementary material of Ref. 20.

We computed state-to-state DCSs with the V_{sum} and V_{dif} potentials given in the work of Kłos *et al.*[21] In the QM CC scattering calculations, we used a channel basis including all partial wave contributions up to total angular momentum $J = 101.5$ and all NO rotational levels up to $j = 15.5$ for collision energies up to 150 cm^{-1}. For the higher collision energies, all total angular momenta up to $J = 200.5$ and all NO rotational levels up to $j = 20.5$ were included. The renormalized Numerov method[22] was used for the propagation of the wavefunctions on a grid from 3.5 to 60 bohr. Cross sections were calculated for collision energies between 14 and 150 cm^{-1} in steps of 1 cm^{-1} and at additional energies between 200 and 700 cm^{-1} in steps of 100 cm^{-1}. At energies around the experimental collision energies, cross sections were calculated on a finer energy grid. The resulting *ab initio* calculated DCSs were then used in simulations that take the kinematics of the experiment into account to produce angular distributions and simulated images that can be directly compared with the measured images.[20,23]

III. RESULTS

We measured scattering images at six different collision energies between 25.9 and 315 cm^{-1}. Figure 1 shows experimental scattering images for the $j = 1/2, f \rightarrow j' = 3/2, e$ (top panels) and $j = 1/2, f \rightarrow j' = 5/2, f$ (bottom panels) transitions at collision energies of 25.9 (left) and 315 cm^{-1} (right) as an example. These images are compared to the simulated images based on the calculated DCSs.

In Fig. 1, it should be noted that the images become smaller with decreasing collision energy since the scattered products get smaller velocities. Moreover, at a collision energy of 25.9 cm^{-1}, the image for the $j' = 5/2, f$ final state is clearly smaller than the image for the $j' = 3/2, e$ final state because of the higher internal energy of the former state which leaves less kinetic energy. At a collision energy of 25.9 cm^{-1}, the angular structures in the images are different for the two parity-pair transitions—especially in the backward direction—while at an energy of 315 cm^{-1}, the two images look very similar.

The similarity of the parity-pair DCSs can be investigated further by inspecting the experimental and simulated angular distributions. Figure 2 compares the experimental (solid curves) and simulated angular distributions (dash-dotted curves) for the $j = 1/2, f \rightarrow j' = 3/2, e$ (blue) and $j = 1/2, f \rightarrow j' = 5/2, f$ (red) transitions at different collision energies. The insets show a comparison between the theoretically predicted DCSs for these transitions that are used as input for the simulations, i.e., before taking into account the kinematics of the experiment. In general, there is very good agreement between the experimental and simulated images and angular distributions. At high collision energies, the two transitions exhibit similar structures in the theoretical DCSs and in both the simulated and experimental angular distributions. When the collision energy is lowered, however, a shift can be observed between the diffraction oscillations in the angular distributions for the two transitions. At collision energies below 40 cm^{-1}, different structures are observed for the two transitions. Clearly, the similarity of the parity-pair DCSs breaks down when the collision energy is reduced.

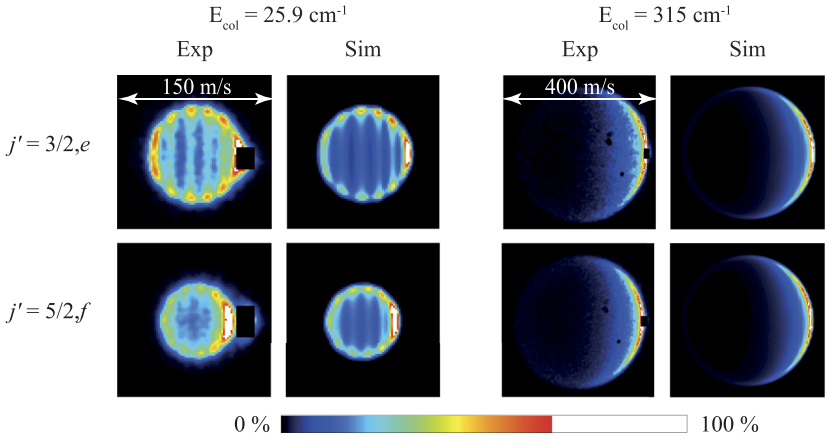

FIG. 1. Experimental and simulated scattering images for the $j = 1/2, f \rightarrow j' = 3/2, e$ (top panels) and $j = 1/2, f \rightarrow j' = 5/2, f$ (bottom panels) transitions at collision energies of 25.9 (left) and 315 cm^{-1} (right). The images are presented such that the relative velocity vector is oriented horizontally, and that the forward direction is on the right side of the image. Small segments around forward scattering are masked by imperfect state selection of the NO molecules. In the images measured at a collision energy of 315 cm^{-1}, small black spots can be observed due to dust particles on the phosphor screen.

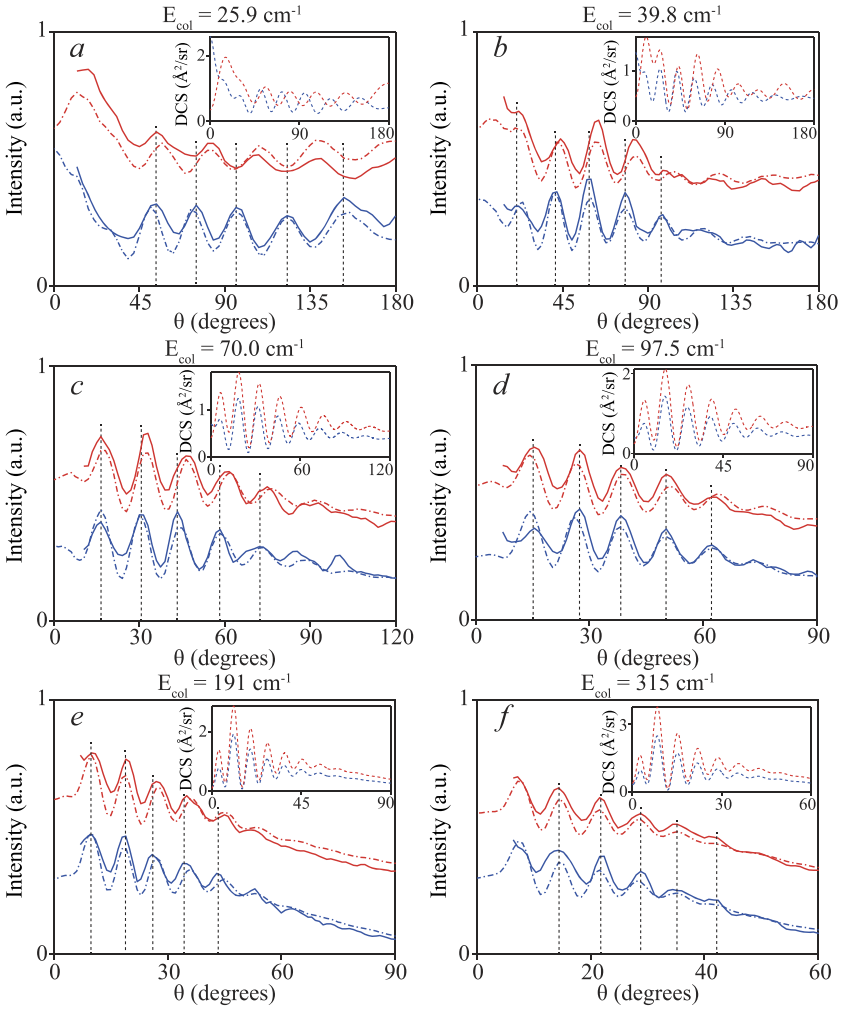

FIG. 2. Experimental (solid curves) and simulated (dash-dotted curves) angular distributions for the $j = 1/2, f \rightarrow j' = 3/2, e$ (blue) and $j = 1/2, f \rightarrow j' = 5/2, f$ (red) transitions at collision energies of 25.9 (a), 39.8 (b), 70.0 (c), 97.5 (d), 191 (e), and 315 cm^{-1} (f). The angular distributions are divided by their Euclidean norm, and the red curves are given a vertical offset for clarity. Note the different scales on the horizontal axes. The peak positions of the first five experimental diffraction peaks for the $j = 1/2, f \rightarrow j' = 3/2, e$ transition are indicated by dashed vertical lines to guide the eye. The insets show the theoretical DCSs for the $j = 1/2, f \rightarrow j' = 3/2, e$ (blue) and $j = 1/2, f \rightarrow j' = 5/2, f$ (red) transitions.

A. Similarity between parity-pair DCSs

To evaluate how the similarity of the DCSs for the parity-pair transitions evolves as a function of collision energy, we compute the root mean square deviation (RMSD) as a function of energy,

$$\mathrm{RMSD} = \sqrt{\frac{\sum_{i=1}^{N}\left(\frac{\mathrm{DCS}_{1,i}}{||\mathrm{DCS}_1||} - \frac{\mathrm{DCS}_{2,i}}{||\mathrm{DCS}_2||}\right)^2}{N}}, \qquad (1)$$

where DCS_1 is the DCS for the $j' = 3/2, e$ final state, DCS_2 is the DCS for the $j' = 5/2, f$ final state, $||\mathrm{DCS}_1|| = \sqrt{\sum_{i=1}^{N} |\mathrm{DCS}_{1,i}|^2}$ is the Euclidean norm of DCS_1, and N is the number of angular steps in the DCS. An angular stepsize of 0.5° was used for the theoretical DCSs at all energies. The stepsize in the experimental and simulated angular distributions varied with the collision energy, depending on the size of the image. To determine the RMSD, the experimental and simulated angular distributions were interpolated on a grid with a stepsize of 0.5°.

The RMSD of the theoretical DCSs is shown as a function of the collision energy by the black solid curve in Fig. 3. The green dots in this figure represent the RMSD of the experimental angular distributions, whereas the blue diamonds are the RMSD of the simulated angular distributions. In general, the theoretical, experimental, and simulated RMSDs show the same trends. The experimental RMSD is larger than the simulated one, which could be due to experimental noise. Moreover, it should be noted that all angles between 0° and 180° are taken into account to determine the theoretical RMSD, while the most forward scattered angles in the experiment and simulation are not taken into account due to the presence of the beamspot resulting from unscattered molecules. The theoretical, experimental, and simulated RMSDs all clearly increase at lower collision energies, reflecting the larger difference between the DCSs for the parity pairs.

For comparison, we also computed the RMSD for the neighboring $j' = 3/2, e$ and $j' = 3/2, f$ final states and for the $j' = 3/2, e$ and $j' = 5/2, e$ final states with the same spectroscopic parity index ϵ, as shown in Fig. 3. Transitions to these final states do not form parity pairs and have rather different DCSs. Indeed, the RMSD for DCSs of parity-pair transitions is much smaller than the RMSD of DCSs for neighboring final states or final states with the same ϵ at high collision energies. At low collision energies, however, the RMSD is similar for all three situations.

B. Parity pairs probing quantum mechanics

At low collision energies, the wave character of the colliding particles plays a crucial role. The dashed red curve in Fig. 3

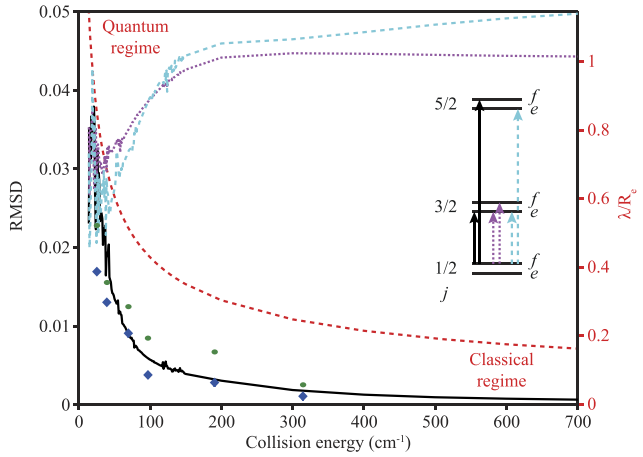

FIG. 3. The similarity of the DCSs for the $j = 1/2, f \rightarrow j' = 3/2, e$ and $j = 1/2, f \rightarrow j' = 5/2, f$ parity-pair transitions is quantified by the RMSD. The theoretical RMSD is shown as a function of the collision energy by the black solid curve, while the green dots and the blue diamonds represent the RMSD of the experimental and simulated angular distributions, respectively. The quantum nature of the system is illustrated by the red dashed line, which represents the ratio between the de Broglie wavelength λ and the equilibrium distance R_e of the NO–He complex. For comparison, the RMSD of the DCSs for the neighboring $j' = 3/2, e$ and $j' = 3/2, f$ final states (purple dotted curve) and the one for the $j' = 3/2, e$ and $j' = 5/2, e$ final states (cyan dashed curve) are shown. Clearly, the DCSs of the parity-pair transitions are much more similar at high collision energies than the DCSs for neighboring final states or final states with the same spectroscopic parity index ϵ.

shows the ratio between the de Broglie wavelength λ and the equilibrium distance $R_e = 3.2$ Å of the NO–He complex. This ratio may be considered as a measure of the quantum nature of the system and increases with lower collision energy. When approaching the quantum regime, the wave character of the colliding particles starts dominating the collision process, and the contributions from the individual partial waves become more important and more clearly visible in the DCS. This is illustrated in Fig. 4, which shows the partial cross sections σ_J for different total angular momenta J for the transition to the $j' = 3/2, e$ (blue dots) and $j' = 5/2, f$ final states (red dots) at collision energies of 25.9 and 500 cm^{-1}. At a collision energy of 500 cm^{-1}, partial waves with total angular momenta around $J = 27.5$ dominate the cross sections, and their relative contributions to the two transitions are similar. Therefore, similar potential matrix elements contribute to the scattering amplitude for the two transitions (see Sec. IV A). However, at a collision energy of 25.9 cm^{-1}, the cross sections are dominated by partial waves with much lower J values, and the contributions of the individual partial waves become important. The largest contribution to the cross section for the $j' = 3/2, e$ state comes from $J = 6.5$ in this case, while the contribution of $J = 6.5$ to the cross section for the $j' = 5/2, f$ state is less important and the maximum contribution instead comes from $J = 5.5$. Clearly, this results in different DCSs.

We also analyzed the contributions from single J values to the DCSs at 25.9 cm^{-1}. We found that the shift between the diffraction oscillations in the DCSs for the $j' = 3/2, e$ and $j' = 5/2, f$ states is reflected by the DCS contributions from $J = 7.5$ and $J = 6.5$, respectively, which is in line with the difference between the J values that give the maximum contributions. However, we also found strong interference between the contributions from different J values so that the total DCSs are not simply the sums of the individual J contributions. The increasing importance of specific partial waves at lower energies is a testimony of the increasing importance of the wave character of the colliding particles. Hence, the parity pairs studied here serve as a measure for the quantum nature of the collision process.

IV. ANALYSIS, BORN MODEL FOR PARITY PAIRS

In order to understand why the DCSs for parity-pair transitions are so similar at high collision energies, we first discuss QM CC calculations in which we only used a specific anisotropic term in the PES. Next, we apply the first-order Born model[24] to calculate the DCSs because this model might explain the similarity of the DCSs. We investigate, in particular, whether the anisotropy of the potential is sufficiently weak for the Born model to be applicable.

A. QM CC calculations with a truncated potential expansion

Let us first identify which part of the PES governs the parity-pair transitions, which are spin-orbit conserving transitions. In the Hund's case (a) limit, which is exact for NO in its $j = 1/2$ state and which is a very good approximation for all low j states, these transitions are determined by the potential $V_{\mathrm{sum}}(R, \gamma) = (V_{A'} + V_{A''})/2$, where $V_{A'}$ and $V_{A''}$ are the adiabatic potentials calculated *ab initio*[21] for the states of NO–He that are symmetric (A') and antisymmetric (A'') on reflection

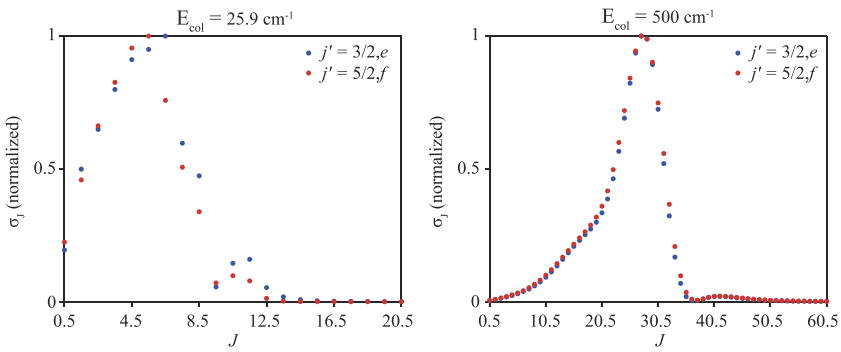

FIG. 4. Partial cross sections for the different total angular momenta J for the $j = 1/2, f \rightarrow j' = 3/2, e$ (blue) and $j = 1/2, f \rightarrow j' = 5/2, f$ (red) parity-pair transitions at collision energies of 25.9 (left) and 500 cm^{-1} (right). The partial cross sections are normalized such that the maximum contribution is 1.

in the plane of the complex. This potential $V_{\rm sum}(R, \gamma)$ can be expanded in terms of Legendre polynomials $P_L(\cos\gamma)$ as

$$V_{\rm sum}(R,\gamma) = \sum_{L=0}^{\infty} V_L(R) P_L(\cos\gamma), \tag{2}$$

where $V_L(R)$ are the expansion coefficients, R is the length of the vector $\mathbf{R}$ that connects the He atom with the center-of-mass of the NO molecule, and γ is the angle between the vector $\mathbf{R}$ and the internuclear axis of NO. Figure 5 shows the expansion coefficients up to $L = 5$ as a function of the distance R.

The potential matrix elements for spin-orbit conserving transitions, i.e., transitions with $\Omega = \Omega'$, are given by[25]

$$\begin{aligned}\langle j'\ell'\Omega\epsilon' JM|V|j\ell\Omega\epsilon JM\rangle &= (-1)^{j+j'+J-\Omega}\sqrt{(2j+1)(2j'+1)(2\ell+1)(2\ell'+1)} \\ &\times \sum_L \begin{pmatrix} \ell' & L & \ell \\ 0 & 0 & 0 \end{pmatrix} \begin{Bmatrix} j & \ell & J \\ \ell' & j' & L \end{Bmatrix} \frac{1}{2}\left[1 - \epsilon\epsilon'(-1)^{j+j'+L}\right] \\ &\times V_L(R) \begin{pmatrix} j' & L & j \\ -\Omega & 0 & \Omega \end{pmatrix}. \end{aligned} \tag{3}$$

Here, j is the total angular momentum of the NO molecule, Ω is the projection of j on the internuclear axis of NO, ℓ is the orbital angular momentum quantum number of the NO–He collision complex, J is the total angular momentum quantum number with space-fixed projection M, and (:::) and {:::} are Wigner $3j$ and $6j$ symbols, respectively. For the initial $j = 1/2$ state, it can be seen from the symmetry factor $\frac{1}{2}[1 - \epsilon\epsilon'(-1)^{j+j'+L}]$ and the $3j$ and $6j$ symbols that transitions to final states j', e and $j' + 1$, f are both directly coupled by the same V_L term in the expansion of the potential. These transitions have the same final parity p' and the same value for n and form a parity pair. The parity-pair transitions investigated here, with final states $j' = 3/2$, e and $j' = 5/2$, f, are both directly coupled to the $j = 1/2$, f initial state by the V_2 term (shown by the red dashed line in Fig. 5).

There is, however, no simple relation between these potential matrix elements and the cross sections. The cross sections are related to the scattering amplitude and, in particular, the DCS is directly given by the square of this scattering amplitude.[26] For a specific $j, m, \Omega, \epsilon \rightarrow j', m', \Omega', \epsilon'$ transition, the scattering amplitude is given by[27]

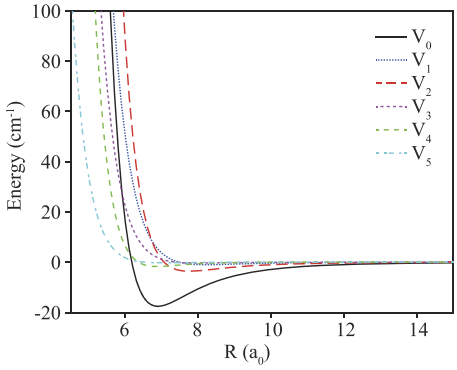

FIG. 5. Plot of the $V_L(R)$ expansion coefficients up to $L = 5$ of the $V_{\rm sum}$ potential energy surface for NO + He as a function of the distance R.

$$\begin{aligned} f_{jm\Omega\epsilon\rightarrow j'm'\Omega'\epsilon'}(\theta) = \sum_{J\ell\ell'} i^{\ell-\ell'}\sqrt{\pi(2\ell+1)}(2J+1) \begin{pmatrix} j & J & \ell \\ m & -m & 0 \end{pmatrix} \\ \times \begin{pmatrix} j' & J & \ell' \\ m' & -m & m'_\ell \end{pmatrix} T^J_{j\ell\Omega\epsilon,j'\ell'\Omega'\epsilon'} Y_{\ell' m'_\ell}(\theta, 0), \end{aligned} \tag{4}$$

where θ is the scattering angle, m and m_ℓ are the space-fixed projections of j and ℓ, respectively, and $T^J_{j\ell\Omega\epsilon,j'\ell'\Omega'\epsilon'}$ is a T-matrix element, which is related to the corresponding S-matrix element by[27]

$$T^J_{j\ell\Omega\epsilon,j'\ell'\Omega'\epsilon'} = \delta_{jj'}\delta_{\ell\ell'}\delta_{\Omega\Omega'}\delta_{\epsilon\epsilon'} - S^J_{j\ell\Omega\epsilon,j'\ell'\Omega'\epsilon'}. \tag{5}$$

The full S matrix can be found after solving the QM CC equations, in which the potential matrix elements of Eq. (3) appear in the so-called W matrix, which describes the R-dependent interaction between the channels.

We investigate the effect of the V_2 term in the Legendre expansion of the potential that directly couples the $j' = 3/2$, e and $j' = 5/2$, f final states to the initial $j = 1/2$, f state by performing QM CC calculations with this term as the only anisotropic contribution to the potential. That is, we use the potential $V_{\rm sum}(R, \gamma) = V_0(R)P_0(\cos\gamma) + V_2(R)P_2(\cos\gamma)$ and put $V_{\rm dif} = 0$. Figure 6 shows the DCSs for the two transitions computed with the full PES (blue) or with the truncated PES (red) at collision energies of 40 and 730 cm^{-1}. It can be seen in this figure that the truncated PES produces the same structures in the DCS as the full PES and only slightly overestimates the DCSs for both transitions and for both collision energies. This demonstrates that the similar behavior of the DCSs of the parity pairs is mainly determined by a single anisotropic term in the potential, both at high and at low collision energies.

B. Born approximation

When the interaction between colliding particles is weak and the interaction potential V only produces a small perturbation of the incident plane wave ψ_a, one can use the Born approximation for the T matrix for a transition from state a to b,[28]

$$T_{a\rightarrow b} \approx T^{\rm Born}_{a\rightarrow b} = \langle\psi_b|V|\psi_a\rangle. \tag{6}$$

The Born approximation in its simplest form uses free-particle wavefunctions as the unperturbed functions, which for our case would lead to

$$T^J_{j\ell\Omega\epsilon,j'\ell'\Omega'\epsilon'} = \langle J_{\ell'}(k_{j'\ell'\Omega'\epsilon'}R)|V|J_\ell(k_{j\ell\Omega\epsilon}R)\rangle, \tag{7}$$

with $J_\ell(k_{j\ell\Omega\epsilon}R)$ being a spherical Bessel function with wavevector $k_{j\ell\Omega\epsilon} = \sqrt{2\mu(E - E_{j\ell\Omega\epsilon})}$. Here, E is the total energy of the system and $E_{j\ell\Omega\epsilon}$ are the energies of the states of the isolated NO molecule. The problem is, however, that free-particle waves extend to $R = 0$, well within the repulsive wall, where the interaction potential becomes very large and a free-particle wave is a bad zeroth order description of the system. So, instead, we apply a generalized Born approximation in which the unperturbed wavefunctions are the solutions $\Psi^0_{j\ell\Omega\epsilon}$ of the Schrödinger equation with

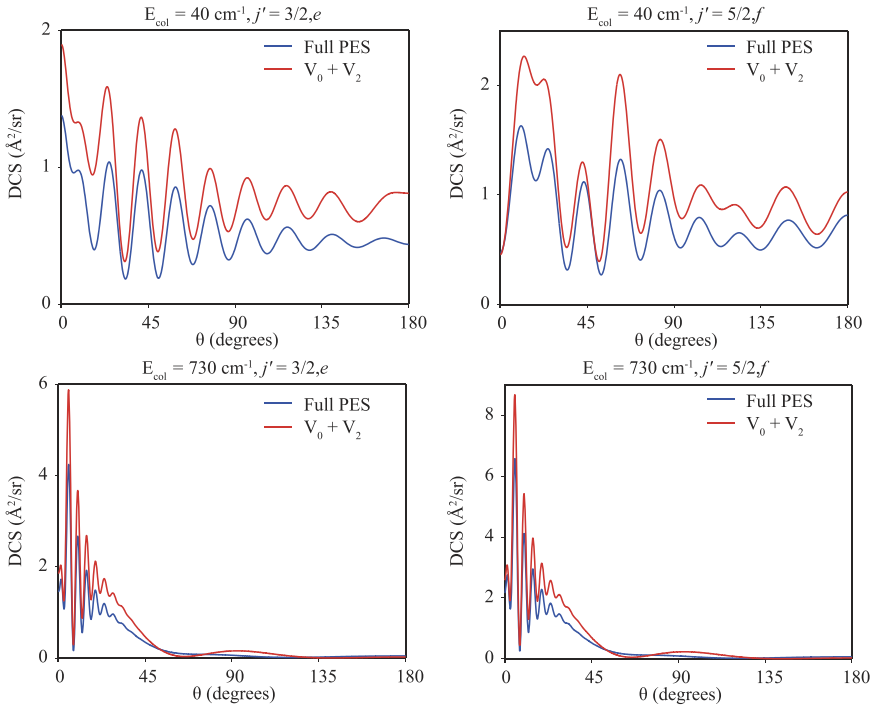

FIG. 6. Theoretical DCSs resulting from QM CC calculations based on the full PES (blue) or a truncated expansion of the potential (red) are shown for the $j = 1/2, f \rightarrow j' = 3/2, e$ (left) and $j = 1/2, f \rightarrow j' = 5/2, f$ (right) parity-pair transitions at collision energies of 40 (top panels) and 730 cm^{-1} (bottom panels).

the interaction potential restricted to the isotropic term V_0 and use the V_2 term as the perturbation. This results in the expression

$$T^J_{j\ell\Omega\epsilon,j'\ell'\Omega'\epsilon'} = \langle \Psi^0_{j'\ell'\Omega'\epsilon'} | V_2(R) P_2(\cos\gamma) | \Psi^0_{j\ell\Omega\epsilon} \rangle. \quad (8)$$

So, when this generalized Born approximation is valid, the potential matrix element in Eq. (3) that directly couples the initial and final states, in this case through the V_2 term, directly determines the scattering amplitude and the DCS. The similarity of the DCSs for parity pairs then follows naturally from the symmetry properties of the potential matrix elements.

The results of our calculations with this generalized Born model are summarized in Table I. In the first line of this table, one can see that when we included the full anisotropic V_2 term in the potential, the integral cross section (ICS) resulting from the Born model calculations is much larger than the ICS resulting from the full QM CC calculations. So, even at a relatively high collision energy of 730 cm^{-1}, where the Born approximation should work best since it is based on perturbation theory, it breaks down. A further inspection revealed that the contributions to the ICS from high total angular momenta J, i.e., large impact parameters where the interaction is weak, are the same but that the contributions strongly deviate for smaller J. To further investigate the validity of the Born approximation, we scaled the V_2 term in the potential by factors ranging from 0.5 to 0.001 such that the anisotropic interaction gets weaker and weaker. For a scaling factor of 0.1, we already obtain reasonable agreement between the QM CC result and the Born model result; for scaling factors of 0.01 and 0.001, we get perfect agreement. One may notice also that the validity of the Born model naturally implies that the ICS becomes proportional to the square of the strength of the anisotropic interaction, i.e., to the square of the scaling factor. In conclusion, the V_2 term in the NO–He interaction potential is too strong for the first-order Born model to be applicable, even at high collision energies. We thus conclude that the idea that the Born model explains the similarity of DCSs for parity pairs must be rejected.

TABLE I. ICSs for the $j = 1/2, f \rightarrow j' = 3/2, e$ transition at a collision energy of 730 cm^{-1}, resulting from QM CC calculations based on a truncated expansion of the potential and from the Born model. For both cases, $V_{sum}(R, \gamma) = V_0(R)P_0(\cos\gamma) + \zeta V_2(R)P_2(\cos\gamma)$ and $V_{dif} = 0$, where ζ is a factor used to scale the anisotropic V_2 term in the potential. The ICS from QM CC calculations with the full interaction potential is 2.28 $Å^2$, which confirms that the truncation of the anisotropy in the potential has only a small effect on this cross section.

ζ	QM CC ($Å^2$)	Born ($Å^2$)
1	3.26	83.5
0.5	4.76	21.0
0.1	0.76	0.84
0.01	0.008 4	0.008 4
0.001	0.000 084	0.000 084

C. Other parity-pair transitions

So far, we only discussed a specific parity-pair transition for collisions between NO radicals and He atoms. Our approach can be extended, however, to different parity-pair transitions and collision partners. As described in Refs. 18 and 19, transitions to higher rotational states of the NO molecule generally involve multiple anisotropic terms in the expansion of the potential and higher-order mechanisms, or the so-called virtual transitions. Hence, the truncation of the potential to the isotropic and a single anisotropic term would not produce a similar DCS as the full potential, as shown in Fig. 6. Moreover, transitions to higher rotational states of the NO

TABLE II. The RMSD for parity-pair transitions with different n values at a collision energy of 300 cm^{-1}.

j'	j'	n	RMSD
1/2, e	3/2, f	1	0.0010
3/2, e	5/2, f	2	0.0019
5/2, e	7/2, f	3	0.0027
7/2, e	9/2, f	4	0.0057
9/2, e	11/2, f	5	0.0033
11/2, e	13/2, f	6	0.0033
13/2, e	15/2, f	7	0.0038

molecule are generally caused by collisions with lower values of J, i.e., smaller impact parameters,[29] resulting in stronger interactions. Therefore, we expect larger differences between the DCSs of the parity-pair transitions for these higher excitations already at relatively high collision energies. This is confirmed by the RMSD values for parity pairs with different n values at a collision energy of 300 cm^{-1}, which are shown in Table II.

V. CONCLUSIONS

We have presented measured and computed DCSs for the so-called parity-pair transitions in collisions between NO radicals and He atoms. Both experimentally and theoretically, we observed a high level of similarity between the DCSs for the parity-pair transitions at high collision energies, as has been observed and computed in earlier studies.[15–19] Here, we could for the first time observe this similarity at the level of diffraction oscillations, which are the narrowest structures occurring in DCSs. At low collision energies, our high experimental angular resolution allowed us to observe a gradually increasing difference between the two DCSs of a parity pair.

In order to understand the mechanism leading to similar DCSs for parity pairs, we performed quantum mechanical close-coupling calculations both with the full anisotropic interaction potential and with only a single anisotropic term in this potential, viz., the V_2 term that directly couples the initial and final states involved in the transition for both members of the parity pair investigated. If this term could be taken into account in the first-order Born approximation, this would directly explain the similar DCSs of the parity pair. We found, however, that the V_2 term is too strong for the Born approximation to be applicable. Hence, we conclude that it is indeed the direct coupling term in the potential that produces the similar DCSs but that one must include this term to higher order to obtain realistic results.

The results summarized above show that parity-pair transitions can be used as a probe for the quantum nature of the collision process. The lower the collision energy, the smaller the number of partial waves that are involved in the collision, and the more important the contributions are from the individual partial waves. This is reflected in the increasing difference between the DCSs for parity-pair transitions when the collision energy is reduced.

ACKNOWLEDGMENTS

This work is part of the research program of the Netherlands Organization for Scientific Research (NWO). The research leading to these results has received funding from the European Research Council under the European Union's Seventh Framework Programme (Grant No. FP7/2007-2013)/ERC Grant Agreement No. 335646 MOLBIL. J.O. acknowledges the Alexander von Humboldt Foundation for a postdoctoral fellowship. The expert technical support by Leander Gerritsen, Chris Berkhout, Peter Claus, Niek Janssen, and André van Roij is gratefully acknowledged.

[1] J. Weiner, V. S. Bagnato, S. Zilio, and P. S. Julienne, Rev. Mod. Phys. **71**, 1 (1999).
[2] *Cold Molecules: Theory, Experiment, Applications*, edited by R. Krems, W. Stwalley, and B. Friedrich (Taylor and Francis, 2009).
[3] M. T. Bell and T. P. Softley, Mol. Phys. **107**, 99 (2009).
[4] L. Carr, D. DeMille, R. Krems, and J. Ye, New J. Phys. **11**, 055049 (2009).
[5] M. Schnell and G. Meijer, Angew. Chem., Int. Ed. **48**, 6010 (2009).
[6] O. Dulieu, R. Krems, M. Weidemuller, and S. Willitsch, Phys. Chem. Chem. Phys. **13**, 18703 (2011).
[7] G. Quéméner and P. S. Julienne, Chem. Rev. **112**, 4949 (2012).
[8] E. S. Shuman, J. F. Barry, and D. DeMille, Nature **467**, 820 (2010).
[9] A. Fioretti, D. Comparat, A. Crubellier, O. Dulieu, F. Masnou-Seeuws, and P. Pillet, Phys. Rev. Lett. **80**, 4402 (1998).
[10] T. Takekoshi, B. M. Patterson, and R. J. Knize, Phys. Rev. Lett. **81**, 5105 (1998).
[11] J. M. Doyle, B. Friedrich, J. Kim, and D. Patterson, Phys. Rev. A **52**, R2515 (1995).
[12] H. L. Bethlem, G. Berden, and G. Meijer, Phys. Rev. Lett. **83**, 1558 (1999).
[13] R. V. Krems, Phys. Chem. Chem. Phys. **10**, 4079 (2008).
[14] G. Quéméner, N. Balakrishnan, and A. Dalgarno, "Inelastic collisions and chemical reactions of molecules at ultracold temperatures," in *Cold Molecules: Theory, Experiment, Applications*, edited by R. Krems, W. Stwalley, and B. Friedrich (Taylor and Francis, 2009), pp. 69–124.
[15] A. Gijsbertsen, H. Linnartz, G. Rus, A. E. Wiskerke, S. Stolte, D. W. Chandler, and J. Kłos, J. Chem. Phys. **123**, 224305 (2005).
[16] A. Gijsbertsen, H. Linnartz, C. A. Taatjes, and S. Stolte, J. Am. Chem. Soc. **128**, 8777 (2006).
[17] A. Ballast, A. Gijsbertsen, H. Linnartz, and S. Stolte, Mol. Phys. **106**, 315 (2008).
[18] J. Kłos, F. J. Aoiz, J. E. Verdasco, M. Brouard, S. Marinakis, and S. Stolte, J. Chem. Phys. **127**, 031102 (2007).
[19] C. J. Eyles, M. Brouard, H. Chadwick, F. J. Aoiz, J. Kłos, A. Gijsbertsen, X. Zhang, and S. Stolte, Phys. Chem. Chem. Phys. **14**, 5420 (2012).
[20] S. N. Vogels, J. Onvlee, S. Chefdeville, A. van der Avoird, G. C. Groenenboom, and S. Y. T. van de Meerakker, Science **350**, 787 (2015).
[21] J. Kłos, G. Chałasiński, M. T. Berry, R. Bukowski, and S. M. Cybulski, J. Chem. Phys. **112**, 2195 (2000).
[22] B. R. Johnson, NRCC Proc. **5**, 86 (1979).
[23] A. von Zastrow, J. Onvlee, S. N. Vogels, G. C. Groenenboom, A. van der Avoird, and S. Y. T. van de Meerakker, Nat. Chem. **6**, 216 (2014).
[24] M. Born, Z. Phys. **38**, 803 (1926).
[25] F. J. Aoiz, J. E. Verdasco, M. Brouard, J. Kłos, S. Marinakis, and S. Stolte, J. Phys. Chem. A **113**, 14636 (2009).
[26] W. A. Lester, Jr., "The N coupled-channel problem," in *Dynamics of Molecular Collisions, Part A* (Plenum Press, New York, USA, 1976), pp. 1–32.
[27] M. H. Alexander, J. Chem. Phys. **76**, 5974 (1982).
[28] A. Messiah, *Quantum Mechanics Volume II* (North Holland Publishing Company, 1965).
[29] J. Onvlee, S. N. Vogels, A. van der Avoird, G. C. Groenenboom, and S. Y. T. van de Meerakker, New J. Phys. **17**, 055019 (2015).